Replica symmetry breaking solution for the fermionic Ising spin-glass and the Ghatak-Sherrington model

2000 J. Phys. A: Math. Gen. 33 1325

(http://iopscience.iop.org/0305-4470/33/7/303)

J. Phys. A: Math. Gen. **33** (2000) 1325–1332. Printed in the UK PII: S0305-4470(00)08177-4

Replica symmetry breaking solution for the fermionic Ising spin-glass and the Ghatak–Sherrington model

H Feldmann and R Oppermann

Institut für Theoretische Physik, Universität Würzburg, Am Hubland, 97074 Würzburg, Germany

E-mail: feldmann@physik.uni-wuerzburg.de

Received 27 September 1999

Abstract. We solve the fermionic version of the Ising spin glass for arbitrary filling μ and temperature T taking into account replica symmetry breaking. Using a simple exact mapping from μ to the anisotropy parameter D, we also obtain the solution of the $S = 1$ Sherrington–Kirkpatrick model. An analytic expression for $T = 0$ gives an improved critical value for the first-order phase transition. We revisit the question of stability against replica-diagonal fluctuations and find that the appearance of complex eigenvalues of the Almeida–Thouless matrix is not an artefact of the replica-symmetric approximation.

1. Introduction and mapping of the two models

A direct generalization of the Sherrington–Kirkpatrick (SK) model [1] to include quantum fluctuations are fermionic spin glasses [2]. They provide a larger class of models, since the partition functions of all classical spin-glass models can be extracted from them through the Popov–Fedotov trick [3, 4]. They also allow one to extend standard spin-glass theory to itinerant systems, to study the influence of spin-glass order on the excitation spectrum [5] and to investigate the competition of spin-glass order with other kinds of ordering typical of quantum systems [6]. All these aspects may be relevant to the physics of heavy-fermion compounds.

Another extension of the SK model is the $S = 1$ spin glass in a crystal field, realized for example in $(Ti_{1-x}V_x)_2O_3$ [7]. Both extensions show tricritical behaviour as the chemical potential μ (for fermionic spin glasses) or the anisotropy parameter D are varied [7, 8]. A simple mapping relates the two models, as far as the static properties are concerned.

The fermionic Ising spin glass (ISG_f) is described by the grand canonical Hamiltonian

$$\mathcal{H} = -\sum_{i<j} J_{ij}\sigma_i\sigma_j - \mu\sum_i n_i. \tag{1}$$

The coupling J_{ij} is Gaussian distributed around 0 with variance J^2. In what follows, we always set $J = 1$. The main difference to the SK spin glass is that spins and occupation numbers are given in terms of fermionic operators which act on a space with four states per site, $|00\rangle$, $|\uparrow 0\rangle$, $|0\downarrow\rangle$, and $|\uparrow\downarrow\rangle$:

$$\sigma = a_\uparrow^\dagger a_\uparrow - a_\downarrow^\dagger a_\downarrow \qquad n = a_\uparrow^\dagger a_\uparrow + a_\downarrow^\dagger a_\downarrow. \tag{2}$$

To obtain the thermodynamic behaviour of the model, we calculate the free energy using the replica trick [9]. Integrating over the distribution of J_{ij} creates eight-fermion correlations,

0305-4470/00/071325+08$30.00

which are decoupled using the Parisi matrix of order parameters $Q^{a\tau,b\tau'}$. For mean-field theory, we use the static saddle point of this matrix. Details of this calculation can be found in [2, 5].

The $S = 1$ anisotropic spin-glass or Ghatak–Sherrington (GS) model [7] is represented by the Hamiltonian

$$\mathcal{H} = -\sum_{i<j} J_{ij} S_{iz} S_{jz} + D \sum_i S_{iz}^2 \tag{3}$$

where S_z may have the values -1, 0, and 1. It is easy to see that the partition function corresponding to the Hamiltonian (1) is identical—apart from the constant $1 + \exp(-2\beta\mu)$—to the one defined by (3), provided one maps anisotropy and chemical potential according to

$$\mathrm{e}^{\beta D} = \mathrm{e}^{\beta\mu} + \mathrm{e}^{-\beta\mu}. \tag{4}$$

As a consequence of (4), the thermodynamic properties of both models are directly related. At $T \to 0$, one may even neglect the last term and set $D = \mu$. Note, however, that there is a whole class of fermionic correlations that cannot be expressed in terms of S_z and are therefore unique to the ISG_f, because their definition requires a fermionic generating functional. A good example is the fermion Green function [10]. Additionally, the Heisenberg and XY variants of the ISG_f, since they exhibit quantum dynamics, do not have a direct classical analogue.

In passing, we note that there is another interesting connection between the two models in addition to the mapping (4) and the above-mentioned Popov–Fedotov method. One could introduce a repulsive Hubbard-like on-site interaction U to Hamiltonian (1), which would deplete the doubly occupied states in the limit of infinite strength. In this case, the Hamiltonian and a mapping similar to (4) would read

$$\mathcal{H} = -\sum_{ij} J_{ij}\sigma_i\sigma_j - \left(\mu - \frac{U}{2}\right)\sum_i n_i + U\sum_i \left(a_\uparrow^\dagger a_\uparrow - \frac{1}{2}\right)\left(a_\downarrow^\dagger a_\downarrow - \frac{1}{2}\right) \qquad \text{and}$$

$$\mathrm{e}^{\beta D} = \mathrm{e}^{-\beta\mu} + \mathrm{e}^{\beta\mu - \beta U}. \tag{5}$$

2. Results at nonzero temperature

It has been known for a long time that the two models under consideration are described by two mean-field parameters, $q(x)$ and the replica-diagonal saddle-point value, $Q^{aa} = \tilde{q}$ (in the notation of the ISG_f).

Already from replica-symmetric (RS) calculations, one can locate the second-order critical line, terminating at the tricritical point at ($T = \frac{1}{3}$, $D = 0.962$ or $\mu = 0.961$). In order to correctly describe the system below this line, one has to allow for replica symmetry breaking (RSB). Since only a few results are available for full RSB [6], the first step of the Parisi scheme (1RSB) [11] can give valuable information. In many cases, it already comes close to the full solution or allows a good conjecture.

Using the standard form of RSB at the one-step level, we use the order parameters $q_1 = q(1)$ and $q_2 = q(0)$. The position of the jump in q is given by m. After integration over the fermionic fields and some other transformations we obtain the replica-broken free energy

$$\beta f = \frac{\beta^2 J^2}{4}((\tilde{q}-1)^2 - (q_1-1)^2 + m(q_1^2 - q_2^2)) - \beta\mu - \frac{1}{m}\int_{z_2}^{G} \ln \int_{z_1}^{G} \mathcal{C}^m \tag{6}$$

with

$$\mathcal{C} = \cosh\left(\beta h + \beta J\sqrt{q_1 - q_2}z_1 + \beta J\sqrt{q_2}z_2\right) + \cosh(\beta\mu)\mathrm{e}^{-\frac{\beta^2 J^2}{2}(\tilde{q}-q_1)}. \tag{7}$$

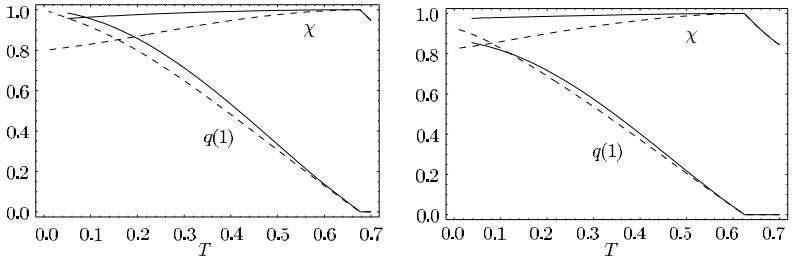

Figure 1. Susceptibility χ and Edwards–Anderson order parameter $q(1)$ for the ISG_f for half-filling (left) and for $\mu = 0.5$ (right). Solid and dashed curves show the results from the one-step replica-broken and the RS solutions, respectively.

The mean-field solutions of the model are given by the condition that f is stationary with respect to $\tilde{q}, q_1, q_2$, and m. Considerable numerical effort is necessary to solve the resulting self-consistency equations for these four parameters simultaneously, and for all values of chemical potential and temperature within the ordered phase. In figure 1 we present a selection of our results, introducing the susceptibility $\chi = \beta(\tilde{q} - (1-m)q_1 - mq_2)$. We compare our results with results from the RS calculation. Note that χ in 1RSB is already very close to the expected exact value $\chi = 1$ in the ordered phase, especially for temperatures close to the phase transition.

3. Zero-temperature results

In the limit of vanishing temperature, $q = \tilde{q} + \mathrm{O}(T)$. Additionally, m vanishes as $T \to 0$. Therefore, for the zero-temperature behaviour of the model, we have to use a new set of parameters in order to avoid divergences in (6). We replace $\beta J(\tilde{q} - q_1)$ by the single-valley susceptibility $\overline{\chi}$ and m by aT. Note that although m, the size of the 'lower step' in $q(x)$, vanishes with the temperature, RSB still has a profound effect on the system.

In these new variables, the limit of (6) can be written as

$$f = \frac{1}{2}J\overline{\chi}(q_1 - 1) + \frac{1}{4}Ja(q_1^2 - q_2^2) - \mu - \frac{J}{a}\int_{z_2}^{G} \ln I \tag{8}$$

where I is given for the case $\mu/J < \overline{\chi}/2$ by

$$\begin{aligned} I = {} & \frac{1}{2}\mathrm{e}^{a\sqrt{q_2}z_2 + \frac{1}{2}a^2(q_1-q_2)}\left(1 + \mathrm{erf}\left(\frac{\sqrt{q_2}z_2 + a(q_1-q_2)}{\sqrt{q_1-q_2}\sqrt{2}}\right)\right) \\ & + \frac{1}{2}\mathrm{e}^{-a\sqrt{q_2}z_2 + \frac{1}{2}a^2(q_1-q_2)}\left(1 + \mathrm{erf}\left(\frac{-\sqrt{q_2}z_2 + a(q_1-q_2)}{\sqrt{q_1-q_2}\sqrt{2}}\right)\right) \end{aligned} \tag{9}$$

and for the case $\mu/J > \overline{\chi}/2$ by

$$\begin{aligned} I = {} & \frac{1}{2}\mathrm{e}^{a\sqrt{q_2}z_2 + \frac{1}{2}a^2(q_1-q_2)}\left(1 + \mathrm{erf}\left(\frac{\sqrt{q_2}z_2 - (\frac{\mu}{J} - \frac{\overline{\chi}}{2}) + a(q_1-q_2)}{\sqrt{q_1-q_2}\sqrt{2}}\right)\right) \\ & + \frac{1}{2}\mathrm{e}^{a(\frac{\mu}{J} - \frac{\overline{\chi}}{2})}\left(\mathrm{erf}\left(\frac{(\frac{\mu}{J} - \frac{\overline{\chi}}{2}) - \sqrt{q_2}z_2}{\sqrt{q_1-q_2}\sqrt{2}}\right) + \mathrm{erf}\left(\frac{(\frac{\mu}{J} - \frac{\overline{\chi}}{2}) + \sqrt{q_2}z_2}{\sqrt{q_1-q_2}\sqrt{2}}\right)\right) \\ & + \frac{1}{2}\mathrm{e}^{-a\sqrt{q_2}z_2 + \frac{1}{2}a^2(q_1-q_2)}\left(1 + \mathrm{erf}\left(\frac{-\sqrt{q_2}z_2 - (\frac{\mu}{J} - \frac{\overline{\chi}}{2}) + a(q_1-q_2)}{\sqrt{q_1-q_2}\sqrt{2}}\right)\right). \end{aligned}$$

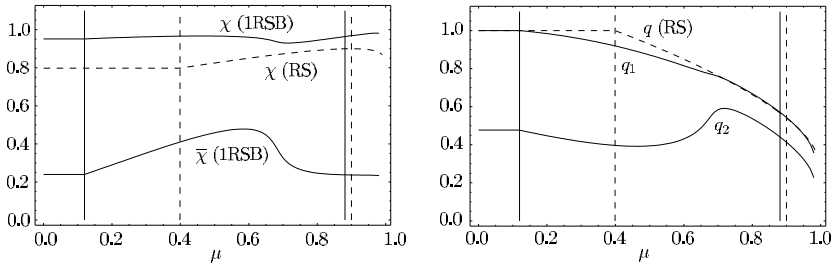

Figure 2. Normal (χ) and single-valley ($\overline{\chi}$) susceptibility (left) and spin-glass order parameters (right) at zero temperature. Solid curves correspond to the replica-broken solution, dashed curves to the RS one. For each case, the left vertical line indicates the onset of the μ-independent solution for small μ, while the right vertical line locates the first-order transition to the paramagnetic regime.

(10)

Again, variation with respect to the order parameters gives four equations describing the saddle-point solution. We solved these for all chemical potentials within the ordered phase and present the results for $\tilde{q} = q_1$, χ and $\overline{\chi}$ in figure 2, together with the RS order parameters for comparison. In RS approximation, $\overline{\chi} = \chi$, which illustrates the importance of RSB.

We also calculated the free energy from (8)–(10) and compared it with the free energy for the paramagnetic phase, $f_{\text{para}} = -2\mu$, to obtain the first-order phase transition at $\mu_{\text{t},1} = 0.881$, a slightly lower value than obtained with the RS approximation, which gave $\mu_{\text{t},0} = 0.900$.

The transition between the two regimes described by (9) and (10) takes place at $\mu = 0.119$, which is also related to the width of the band gap at half-filling [5, 10].

4. RSB in charge correlations

As sections 2 and 3 show, RSB has a profound effect on the low-temperature phase. However, spin and charge correlations are affected differently. While spin correlations are modified by RSB within the whole ordered phase (see the susceptibility in figures 1 and 2), charge correlations remain essentially unchanged by RSB within part of the phase diagram.

The most obvious observable parameter connected to the replica-diagonal order parameter $\tilde{q}$ is the filling ν. Both are related to all orders of RSB by

$$\tilde{q} = 1 - \coth(\beta\mu)(\nu - 1). \tag{11}$$

Zero-temperature results for ν are displayed in figure 3. The difference between the broken and the unbroken solution is largest at the point where the RS value of ν turns constant. Around $\mu = 0.7$, the 1RSB solution bends around to come close to the RS one and the two solutions cross. However, the difference stays comparatively small, so for large μ the filling is virtually unaffected by RSB. A similar situation appears in the standard spin-glass theory for $m > 1$ component spin glasses. There, in a strong magnetic field two characteristic lines appear, first the Gabay–Toulouse line [12–14], where RSB appears for the order parameter perpendicular to the field while it has little effect on the longitudinal order parameter. At a lower temperature, close to the line found by de Almeida and Thouless (AT), the longitudinal order parameter also strongly feels RSB. In this context, one may view the charge and spin degrees of freedom to be 'orthogonal' and the chemical potential to correspond to a magnetic field.

For nonzero temperatures, the difference between RS and 1RSB in general is smaller than for $T = 0$, as shown in figure 4. The merging of the two curves becomes smoother

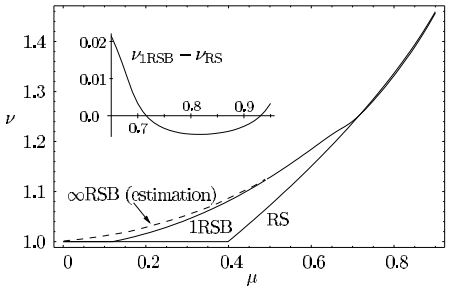

Figure 3. μ-dependence of the filling at zero temperature in the RS and 1RSB approximations. For $\mu < 0.119$, both approximations yield a constant ν, while the full solution, estimated with the dashed curve, gives $\nu = 1$ only at $\mu = 0$. Note the remarkable drop of the RSB solution to the RS curve around $\mu = 0.7$. After the crossing the two curves stay close together. The inset shows the difference between the 1RSB and the RS solutions for large μ.

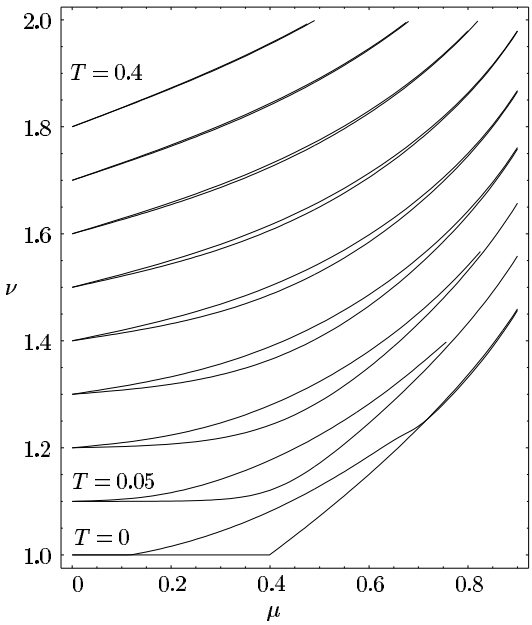

Figure 4. Filling factor ν as a function of the chemical potential for temperatures $T = 0, 0.05, 0.1, \ldots, 0.4$. For each pair of curves, the lower one gives the RS solution, the upper one the 1RSB result. We applied an offset in steps of 0.1 to separate the results for different T. For $\mu = 0$, there is always half-filling. Note that the effect of RSB on $\nu(\mu)$ is significant only in a intermediate range of chemical potentials and for small temperatures.

with increasing temperature. The effect of broken RS on ν is already invisible at $T = 0.4$ in figure 4, far below the second-order phase transition (see figure 5).

For the GS model, the results of this section on the filling can be directly translated to the average number of sites with $S_z = 0$:

$$\tilde{q} = \langle S_z^2 \rangle \qquad \text{or} \qquad \langle 1 - S_z^2 \rangle = \coth(\beta\mu)(\nu - 1). \tag{12}$$

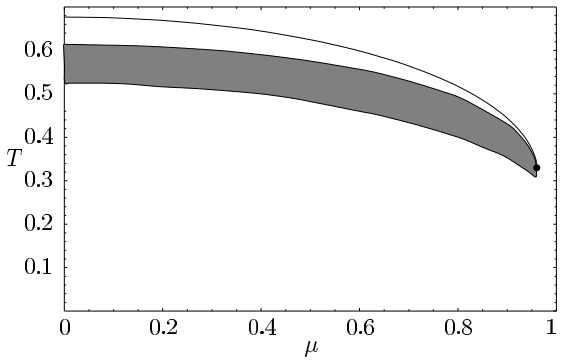

Figure 5. Region of complex replica-diagonal AT eigenvalues in the RS approximation. Also shown is the curve of continuous transitions ending in the tricritcal point.

5. Replica-diagonal stability

The RS solution is unstable against RSB, as shown by AT in [15]. This problem, together with its well known solution using an ultrametric saddle-point matrix [9], is one of the main reasons for the enormous theoretical interest in spin glasses over the past decades.

In addition to the eigenvalue that marks the onset of RSB, AT obtained two additional pairs of eigenvalues which merge in the replica limit. For the SK model, these were positive for all temperatures and did not pose a problem. In the case of the GS model and the ISG$_f$, however, the replica-diagonal eigenvalues can become complex, as noted by several authors [5, 16–18].

This result is very difficult to interpret. Lage and de Almeida [16] derived another set of stability conditions and found their condition $\partial^2 f/\partial \tilde{q}^2$ to be violated at low temperatures, in a region determined by the 'crossover line' of [6]. Mottishaw and Sherrington [17] pointed out that the system is unstable against RSB and they suspected that the full Parisi solution will have only real eigenvalues again.

We have numerically evaluated the self-consistency equations from [2] within the ordered phase and calculated the replica-diagonal eigenvalues. Directly below the second-order phase transition and at low temperatures, they are real and positive, indicating stability against replica-diagonal fluctuations. However, in between there is a region extending from $\mu = 0$ to the tricritical point, where they have an imaginary part, while the real part remains positive (see figure 5). At half-filling, the complex eigenvalues occur between $T = 0.53$ and 0.61.

To extend the AT analysis of the replica-diagonal eigenvalues to RSB, we start with the ansatz for the eigenvector

$$\mu = \begin{pmatrix} \{\epsilon^{(aa)}\} \\ \{\eta^{(ab)}\} \end{pmatrix} \tag{13}$$

where the replica indices run from $a, b = 1$ to n, and only pairs with $a < b$ are considered for $\eta^{(ab)}$. For k-step RSB, the replica-diagonal eigenvector of AT can be generalized to

$$\epsilon^{(aa)} = \alpha \qquad \text{and} \qquad \eta^{(ab)} = \begin{cases} \beta_1 & \text{if} \quad Q^{ab} = q_1 \\ \beta_2 & \text{if} \quad Q^{ab} = q_2 \\ \dots & \\ \beta_{k+1} & \text{if} \quad Q^{ab} = q_{k+1}. \end{cases} \tag{14}$$

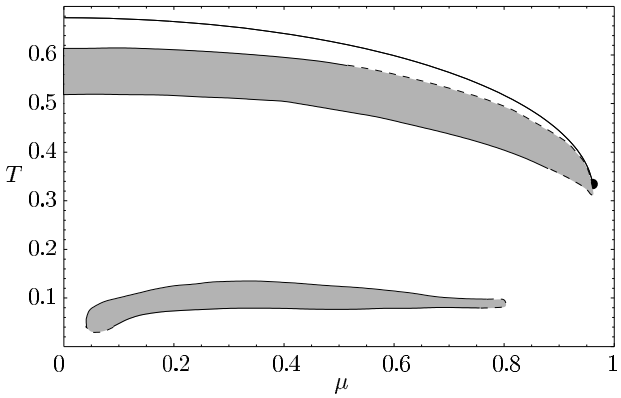

Figure 6. The grey regions show complex AT eigenvalues in one-step RSB. Dashed boundaries indicate difficulties in the numerical algorithm. Here, the true boundary may be slightly shifted.

Substituting (14) into the quadratic form

$$\mu^T G \mu \qquad \text{with} \quad G^{(ab)(cd)} = \frac{\partial}{\partial Q^{ab}} \frac{\partial}{\partial Q^{cd}} f \tag{15}$$

yields $k+2$ replica-diagonal eigenvalues. In the limit of $n \to 0$, these eigenvalues can also be represented as the eigenvalues of a matrix of (much smaller!) size $k+2$:

$$\mathcal{M}_k = \begin{pmatrix} f'' & \dot{f}'_1 & \cdots & \dot{f}'_{k+1} \\ \frac{-2}{(1-m_1)}\dot{f}'_1 & \frac{-2}{(1-m_1)}\ddot{f}_{11} & & \frac{-2}{(1-m_1)}\ddot{f}_{1(k+1)} \\ \frac{-2}{(m_1-m_2)}\dot{f}'_2 & \frac{-2}{(m_1-m_2)}\ddot{f}_{21} & & \frac{-2}{(m_1-m_2)}\ddot{f}_{2(k+1)} \\ \vdots & & \ddots & \vdots \\ \frac{-2}{(m_{(k-1)}-m_k)}\dot{f}'_k & \frac{-2}{(m_{(k-1)}-m_k)}\ddot{f}_{k1} & \cdots & \frac{-2}{(m_{(k-1)}-m_k)}\ddot{f}_{k(k+1)} \\ \frac{-2}{m_k}\dot{f}'_{(k+1)} & \frac{-2}{m_k}\ddot{f}_{(k+1)1} & \cdots & \frac{-2}{m_k}\ddot{f}_{(k+1)(k+1)} \end{pmatrix}. \tag{16}$$

Here, we have introduced the shorthand notations

$$f'' = \frac{\partial^2 f}{\partial \tilde{q}^2} \qquad \dot{f}'_i = \frac{\partial}{\partial q_i}\frac{\partial f}{\partial \tilde{q}} \qquad \text{and} \qquad \ddot{f}_{ij} = \frac{\partial}{\partial q_i}\frac{\partial f}{\partial q_j}. \tag{17}$$

We have carried out the above calculations numerically for 1RSB with the order parameters presented in section 2. Regions with complex replica-diagonal eigenvalues are shown in figure 6. Now there appear two of them. Since f and its derivatives are real, obviously complex eigenvalues always have to appear in pairs conjugate to each other. Labelling the three eigenvalues at 1RSB in proper order, we find that in the high-temperature region of figure 6 $\lambda_1$and λ_2 turn complex, while in the low-temperature region λ_2 and λ_3 have nonzero imaginary parts. Therefore, the two regions can be clearly distinguished. The high-temperature region has approximately the same shape as the one from RS calculations. Its boundary at $\mu = 0$ is given by $T = 0.52$ and $T = 0.61$. This fact is a strong indication that the effect of RSB is small in the corresponding temperature range and that the occurance of complex AT eigenvalues continues for arbitrary RSB. Complex eigenvalues thus seem to be a consequence of the replica limit. Their interpretation as far as stability is concerned remains an open question.

6. Conclusion

Using the equivalence of the thermodynamic properties of the GS model and the fermionic quantum Ising spin glass, we simultaneously solved these two models in the first step of the RS approximation combining analytical and numerical methods. We also obtained the $T = 0$ limit of these solutions. As expected, the effects of RSB are comparatively large in general, while the order parameters of charge are almost unchanged by RSB in certain regions of the ordered phase. Analysing the replica-diagonal AT eigenvalues, we found that the puzzling complex stability eigenvalues, previously found in RS calculations, also appear in one-step RSB. They even cover a larger part of the phase diagram. On this basis, we formulated the conjecture that complex eigenvalues of the stability matrix appear at any order of RSB.

Acknowledgments

This work was supported by the DFG project Op28/5-1, by the SFB410 and by the Villigst foundation.

References

[1] Sherrington D and Kirkpatrick S 1975 *Phys. Rev. Lett.* **35** 1792
[2] Oppermann R and Müller-Groeling A 1993 *Nucl. Phys.* B **401** 507
[3] Popov V N and Fedotov S A 1988 *Zh. Eksp. Teor. Fiz.* **94** 183 (Engl. Transl. 1988 *Sov. Phys.–JETP* **67** 535)
[4] Veits O, Oppermann R, Binderberger M and Stein J 1994 *J. Physique* I **4** 493
[5] Oppermann R and Rosenow B 1999 *Phys. Rev.* B **60** 10 325
[6] Feldmann H and Oppermann R 1999 *Eur. Phys. J.* B **10** 429
[7] Ghatak S K and Sherrington D 1977 *J. Phys. C: Solid State Phys.* **10** 3149
[8] Rosenow B and Oppermann R 1996 *Phys. Rev. Lett.* **77** 1608
[9] Mézard M, Parisi G and Virasoro M A 1987 *Spin Glass Theory and Beyond* (Singapore: World Scientific)
[10] Oppermann R and Rosenow B 1998 *Phys. Rev. Lett.* **80** 4767
[11] Parisi G 1980 *J. Phys. A: Math. Gen.* **13** 1101
[12] Gabay M and Toulouse G 1981 *Phys. Rev. Lett.* **47** 201
[13] Moore M A and Bray A J 1982 *J. Phys. C: Solid State Phys.* **15** L301
[14] Cragg D M, Sherrington D and Gabay M 1982 *Phys. Rev. Lett.* **49** 158
[15] de Almeida J and Thouless D 1978 *J. Phys. A: Math. Gen.* **11** 983
[16] Lage E J S and de Almeida J R L 1982 *J. Phys. C: Solid State Phys.* **15** L1187
[17] Mottishaw P and Sherrington D 1985 *J. Phys. C: Solid State Phys.* **18** 5201
[18] da Costa F A, Yokoi C S O and Salinas S R A 1994 *J. Phys. A: Math. Gen.* **27** 3365